Available online at www.sciencedirect.com

ScienceDirect

Neuromuscular Disorders 28 (2018) 427–442

www.elsevier.com/locate/nmd

# Low dystrophin levels are insufficient to normalize the neuromuscular synaptic abnormalities of *mdx* mice

Elizabeth M. van der Pijl [a], Maaike van Putten [b], Erik H. Niks [a], Jan J.G.M. Verschuuren [a], Annemieke Aartsma-Rus [b], Jaap J. Plomp [a,*]

[a] *Department of Neurology, Leiden University Medical Center, Leiden, The Netherlands*

[b] *Department of Human Genetics, Leiden University Medical Center, Leiden, The Netherlands*

Received 6 October 2017; received in revised form 15 December 2017; accepted 26 February 2018

**Abstract**

Dystrophin is a sub-sarcolemmal component of skeletal muscle fibres and is enriched at the postsynaptic membrane of the neuromuscular junction (NMJ). In the *mdx* mouse, dystrophin absence not only causes muscle damage but also mild synaptic dysfunctions and clear morphological aberrations at NMJs. In particular, reduction of postsynaptic sensitivity for the neurotransmitter acetylcholine and extra exhaustion of presynaptic acetylcholine release during intense synaptic activity exists. Current experimental therapeutic approaches in Duchenne muscular dystrophy aim to restore dystrophin expression. An important question is what dystrophin levels are needed to improve muscle function. Recent experimental and clinical studies suggested that levels as low as a few percent of normal can be beneficial. Similarly, it is of interest to know how dystrophin levels relate to NMJ function and morphology. We investigated NMJs of a series of *mdx-Xist*$^{Ahs}$ mice, which expressed dystrophin between ~2% and 19% of normal. Most functional and morphological NMJ parameters of these mice remained comparable to *mdx*. On the other hand, *mdx*$^{+/-}$ mice (expressing ~50% dystrophin) showed normal NMJ features. Thus, the minimal dystrophin level required for normal NMJ function and morphology lies between 19% and 50% of normal when expression of dystrophin is not uniform.



*Keywords:* Acetylcholine receptor; Duchenne muscular dystrophy; Dystrophin; *mdx* mice; Neuromuscular junction; Synaptic transmission

## 1. Introduction

Duchenne muscular dystrophy (DMD) is an X-linked myopathy caused by the deficiency of dystrophin, a protein important for the stabilization of skeletal muscle fibres [1]. Dystrophin connects intracellular actin to the dystrophin-associated glycoprotein complex and protects against membrane damage from muscle contraction [2].

Dystrophin is also important in the neuromuscular junction (NMJ), where it is enriched at the postsynaptic membrane [3]. In *mdx* mice, which lack dystrophin and display muscle weakness, NMJs show mild neuromuscular synaptic dysfunction and clear morphological deviations. We and others previously showed reduction of postsynaptic sensitivity for the neurotransmitter acetylcholine (ACh) and extra exhaustion of presynaptic ACh release during intense synaptic activity, causing a reduced safety factor of neuromuscular transmission [4,5]. These functional changes are associated by fragmentation of the postsynaptic ACh receptor (AChR) cluster area [5,6]. DMD patients may have similar NMJ abnormalities, indicated by an increased sensitivity to the AChR blocker d-tubocurarine and the prolonged duration of its effect, as compared to healthy controls [7–11].

Therapies aiming to restore dystrophin expression in DMD are currently under investigation [12,13]. Antisense oligonucleotides have been designed which restore the mRNA reading frame through exon-skipping so that internally deleted, but partly functional dystrophin protein is produced. In this way *mdx* mice have been successfully treated to produce dystrophin with an associated improvement of muscle strength [14,15]. Recent studies in DMD patients suggested slowing of disease progression [16,17]. An exon 51 skipping oligonucleotide has received accelerated approval from the US Food and Drug

* Corresponding author. Leiden University Medical Center, Dept. Neurology and MCB Neurophysiology, Research Building, S5-P, P.O. Box 9600, Leiden 2300 RC, The Netherlands.

*E-mail address:* j.j.plomp@lumc.nl (J.J. Plomp).

https://doi.org/10.1016/j.nmd.2018.02.013

Administration based on detected dystrophin levels of <1% of normal, although additional studies were requested to confirm functional effects [18].

An important question arising in relation to these therapeutic studies is what level of dystrophin expression is minimally needed to stop muscle degeneration or even restore function. Female DMD carriers, heterozygous for the *DMD* mutation, are mostly asymptomatic and express ~50%–65% of normal dystrophin protein [19–21]. However, some of them express (considerably) less than 50% dystrophin due to skewed X-inactivation and display clear symptoms of muscle weakness [21,22]. This suggests that at least 50% dystrophin is necessary to support muscle function. On the other hand, in exon-skipped *mdx* mice, a dystrophin level of 15% of normal was shown to protect against muscle damage by forced eccentric contractions [23]. Higher levels of 40%–80% dystrophin in addition caused improvement of basal muscle force as assessed in contraction experiments. Other studies in *mdx*$^{3cv}$ mice and in heterozygous female *mdx* mice with low dystrophin levels due to transgenically induced skewness of X-inactivation revealed that levels of (near full-length or full-length) dystrophin as low as ~5%–15% of normal already improved muscle function [24,25].

In the present study we investigated whether low levels of dystrophin have a beneficial role on the functional and morphological deviations at NMJs of *mdx* mice, which we reported recently [5]. To this end, *mdx* male mice were cross-bred with females homozygous for a mutation in the promoter of the *Xist* gene, which coordinates X-inactivation [26]. Their female *mdx*-*Xist*$^{\Delta hs}$ offspring expresses variable (but always low) full-length dystrophin levels, as a consequence of preferred inactivation of the wild-type X chromosome [25]. NMJ function and morphology of these mice were assessed and compared to that of heterozygous female *mdx* mice (*mdx*$^{+/-}$), which express around 50% of normal dystrophin level [27,28], and homozygous female *mdx* mice.

## 2. Materials and methods

### 2.1. Animals

Female *mdx*-*Xist*$^{\Delta hs}$ mice, expressing variable low levels of dystrophin were investigated. They were compared to groups of female *mdx* and *mdx*$^{+/-}$ mice. The *mdx*-*Xist*$^{\Delta hs}$ mice were obtained through crossing *mdx* male mice with homozygous *Xist*$^{\Delta hs}$ female mice, which carry a mutation in the *Xist* promoter that coordinates X-inactivation [25,26]. Due to the cross-breeding, *mdx*-*Xist*$^{\Delta hs}$ mice had a mixed genetic background of the C57BL/10ScSnJ and the *Xist*$^{\Delta hs}$ mice. We also included females of both these control strains in our comparisons in view of possible strain differences in NMJ parameters. C57BL/10ScSnJ and homozygous *Xist*$^{\Delta hs}$ female mice are assumed to express 100% dystrophin. We used mice of 2–5 months of age. All strains studied were bred at the animal facility of the Leiden University Medical Center. Mice were housed in individually ventilated cages at 20.5 °C with 12-h light-dark cycles and had *ad libitum* access to standard RM3 chow (SDS, Essex, UK) and drinking water. All animal experiments were approved by the Animal Ethics Committee of the Leiden University Medical Center.

### 2.2. In vivo *neuromuscular performance tests*

Respiratory rate and amplitude were assessed with non-invasive whole-body plethysmography in unrestrained animals (RM-80, Columbus Instruments, Columbus, USA). The respiration signal was recorded for 120 s after 30 s acclimatization. The signal was digitized using a Minidigi digitizer and Axoscope 10 software (Axon Instruments/Molecular Devices, Sunnyvale, USA) and analysed with the event detection feature of the Clampfit 10 program (Axon Instruments/Molecular Devices).

The inverted mesh hanging test was used to assess fatigability of limb and abdominal muscles. To this end, mice were placed on an inverted grid forcing mice to hang using all four limbs. The mice were allowed three attempts to hang for a maximum of 240 s. If this maximal hang time was accomplished, the test was stopped. Otherwise the longest hanging time of the three attempts was used for analysis.

Forelimb grip strength was measured with a grip strength meter (type 303500, TSE Systems, Bad Homburg, Germany). Holding the mice at the base of the tail, they were allowed to grasp the pulling bar and were then gently pulled backwards until they released. Ten successive pulls were done with a few seconds pause in between. The mean value was divided by the body weight to obtain the normalized grip strength (g force per g body weight).

Compound muscle action potentials (CMAPs) during repetitive sciatic nerve stimulation-electromyography were recorded from the left calf muscles of ketamine/medetomidine anaesthetized mice as described previously [5].

After completing the electromyography recordings, before recovery from anaesthesia, mice were killed by carbon dioxide inhalation. Diaphragm and epitrochleoanconeus (ETA) muscles were quickly dissected for the electrophysiological and morphological studies described below. Dissected muscles were placed in Ringer's medium at room temperature (20–22 °C), containing (in mM): NaCl 116, KCl 4.5, $CaCl_2$ 2, $MgCl_2$ 1, $NaH_2PO_4$ 1, $NaHCO_3$ 23, glucose 11, pH 7.4, bubbled with a 95% $O_2$ and 5% $CO_2$ gas mixture.

### 2.3. Ex vivo *neuromuscular junction electrophysiology*

Intracellular recordings of endplate potentials (EPPs) and miniature EPPs (MEPPs) at the NMJ were made in Ringer's solution at 26–28 °C in right phrenic nerve-hemidiaphragm preparations. Muscle fibres were impaled near the NMJ with the tip of a glass micro-electrode (5–20 MΩ, filled with 3 M KCl) connected to a Geneclamp 500B (Axon Instruments/Molecular devices, Sunnyvale, CA, USA) for signal amplification and filtering (10 kHz low pass). In each muscle, 40 muscle fibres were impaled to determine the percentage of NMJs that were synaptically active or 'silent' (i.e. showing no MEPPs for at least one min, and no muscle action potential upon subsequent nerve stimulation). Thereafter, muscle action potentials were eliminated by using the skeletal

muscle $Na^+$ channel blocker, μ-Conotoxin-GIIIB (3 μM, PeptaNova, Sandhausen, Germany). For EPP recording, the phrenic nerve was first stimulated with electrical pulses of 0.3 Hz from a computer-controlled programmable stimulator (AMPI, Jerusalem, Israel). Thereafter, MEPPs were sampled during a one min recording period, followed by a train of 35 EPPs that were recorded at 40 Hz nerve stimulation. Within the muscle, 10–15 NMJs were randomly sampled in this way from all mice, except for the muscles of *mdx-Xist*$^{\Delta hs}$ mice, in which 15–34 NMJs were sampled. The signal was digitized using a Digidata 1322A (Axon Instruments/Molecular Devices) digitizer in combination with the Clampfit 9.2 program (Axon Instruments/Molecular Devices). Off-line analysis was done using Mini Analysis 6.0.3 (Synaptosoft, Fort Lee, USA). Mean EPP and MEPP amplitudes at each NMJ were normalized to −75 mV resting potential, assuming a reversal potential of 0 mV. The normalized EPP amplitudes were corrected for nonlinear summation according to Ref. [29] with an *f* value of 0.8. Quantal content, i.e., the number of ACh quanta released per nerve impulse, was calculated by dividing the normalized and corrected mean EPP amplitude by the normalized mean MEPP amplitude at each NMJ.

### 2.4. Ex vivo *muscle contraction studies*

Twitch and tetanic muscle contraction force of the contralateral left phrenic nerve hemidiaphragm preparation was measured *ex vivo* upon single or 40 Hz repetitive (280 pulses, i.e. 7 s duration) supramaximal electrical stimulations, respectively, of the phrenic nerve. Individual pulse duration was 100 μs. Measurements were done in Ringer's medium at room temperature (20–22 °C), continuously bubbled with 95% $O_2$ and 5% $CO_2$, in the presence of increasing concentrations of d-tubocurarine (Sigma-Aldrich, Zwijndrecht, the Netherlands), as described before [5]. The peak amplitude of the recorded twitch contraction and the amplitude of tetanic contractions at 2 s after the start were determined with the Axoscope program (Axon Instruments/Molecular Devices, Sunnyvale, USA).

### 2.5. *Immunohistochemistry and morphological analysis of neuromuscular junctions*

A strip of the right hemidiaphragm and the left ETA of each mouse were fixed in 1% paraformaldehyde in PBS at room temperature for 30 min. To prevent non-specific antibody binding, the tissue was incubated with blocking solution containing 5% normal horse serum and, for permeabilization, 0.5% Triton X-100 in PBS for 45 min. The tissue was incubated overnight at room temperature with dystrophin antibody (C-20, dilution 1:25, Santa Cruz, Germany). After washing with PBS, muscles were incubated for 2.5 h with 1:1000 Alexa Fluor 594-conjugated donkey anti-goat IgG and (to stain AChRs) 1 μg/ml Alexa Fluor 488 conjugated α-bungarotoxin (α-BTx), both from Life Technologies Europe BV, Bleiswijk, The Netherlands. This was followed by thorough PBS/Triton X-100 wash for 30 min at room temperature. Muscle strips were mounted on microscope slides with ProLong Gold antifade mounting medium (Life Technologies Europe BV), and left to harden overnight in the dark at room temperature. The next day, samples were viewed under a Leica TCS STED CW confocal laser scanning microscope using a 40× oil immersion objective. A 387.5 × 387.5 μm overview picture was taken from the NMJ-rich midline zone of each sample. AChR staining area was quantified using the thresholding feature of the ImageJ v1.48k program (http://rsbweb.nih.gov/ij/) at ten randomly chosen NMJs within maximal projections of z-stacks. For each NMJ, the total stained AChR area and the number of discrete AChR islets (as indicator for the amount of fragmentation) were determined.

### 2.6. *Dystrophin level determination*

After electrophysiological analysis, the remaining part of the right hemidiaphragm muscles of all *mdx-Xist*$^{\Delta hs}$ mice was snap frozen in liquid nitrogen and stored for later analysis at −80 °C. After thawing, samples were homogenized and protein concentration was determined using the BCA protein assay kit (Thermo Fischer Scientific, The Netherlands). Dystrophin levels were determined by western blot using the Trans-Blot Turbo system (Bio-Rad, Veenendaal, The Netherlands) according to the protocol of Hulsker et al. [30]. Pooled lysates isolated from tissues from the C57BL/10ScSnJ wild-type controls were used as 100% dystrophin control. For the generation of a calibration curve, serial dilutions of this material were made in *mdx* lysates to ensure equal loading of total protein in each lane. Membranes were stained with NCL-DYS1 for dystrophin (1:125, Novocastra, UK) and alpha actinin (1:7500, AB72592, Abcam, UK) as loading control overnight. The fluorescent IRDye 800CW goat-anti-mouse IgG and IRDye 680LT goat-anti-rabbit IgG (1:5000 and 1:10000 respectively, Li-Cor, USA) were used as secondary antibodies. Blots were visualized and quantified with the Odyssey system and software (Li-Cor).

### 2.7. *Statistical analyses*

Data is presented as means ± SEM in each genotype group, with N as number of mice. In *ex vivo* electrophysiological and fluorescence microscopical analyses, 10–15 NMJs were sampled per muscle in all mice except the *mdx-Xist*$^{\Delta hs}$ mice where 15–34 NMJs were sampled. Per NMJ, 20 EPPs at 0.3 Hz and the MEPPs during a 1 min recording period were sampled. Statistical significances were assessed using ANOVA, and Tukey's honestly post hoc test in case of a statistically significant ANOVA test. The differences in mean data from the two groups of *mdx-Xist*$^{\Delta hs}$ mice with dystrophin levels lower than 6% or higher than 6% were statistically tested with Student's t-test. To assess a possible dependence of the obtained parameters in *mdx-Xist*$^{\Delta hs}$ mice on the dystrophin levels, linear regression was performed and it was tested whether the slope of the fitted line deviated statistically significantly from zero. All statistical analyses were performed using GraphPad Prism 6 (GraphPad Software, Inc. La Jolla, CA, USA); differences with *P*-values $<0.05$ were considered statistically significant. If a statistically significant difference was found, this is indicated in the graphs, together with the obtained *P*-value.

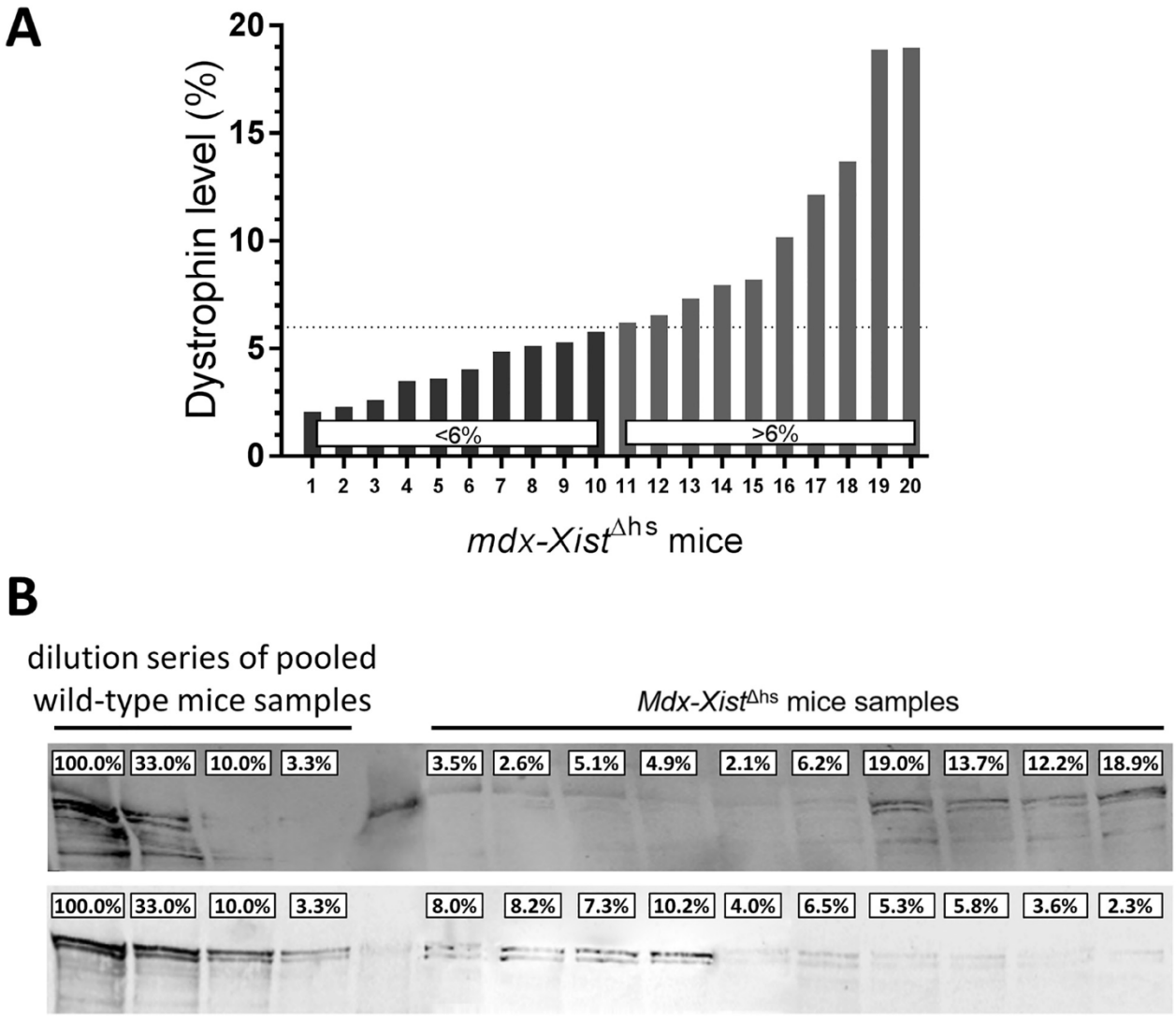


Fig. 1. Distribution of the dystrophin levels. (A) Skewed X-inactivation in the 20 female *mdx-Xist*$^{\Delta hs}$ mice, aged 2–5 months, resulted in individually variable and low dystrophin levels of 2%–19%, as determined by western blot in diaphragm muscle extracts. The group was divided into two sub-sets of mice with dystrophin levels of <6% or >6%, respectively. (B) Two examples of western blots from the dystrophin quantification assays on diaphragm protein lysates of *mdx-Xist*$^{\Delta hs}$ mice. The percentage of dystrophin was determined for each individual mouse using a calibration curve based on a dilution series made from pooled C57BL/10ScSnJ wild-type lysate. Per *mdx-Xist*$^{\Delta hs}$ mouse, 3–6 technical replicates were performed.

## 3. Results

To investigate whether low dystrophin levels prevent NMJ deviations in dystrophic muscle, female *mdx* (0% dystrophin), *mdx-Xist*$^{\Delta hs}$ (variable, low percentages dystrophin), *mdx*$^{+/-}$ (~50% dystrophin), and two control strains (C57BL/10ScSnJ and *Xist*$^{\Delta hs}$, both 100% dystrophin) were studied. Western blot analysis of the dystrophin levels in diaphragm muscle of the 20 *mdx-Xist*$^{\Delta hs}$ studied mice revealed that the levels were low, varying between ~2% and ~19% of normal (Fig. 1). The group average was 7.5% ± 1.1%. Based on the distribution of the dystrophin levels of individual *mdx-Xist*$^{\Delta hs}$ mice, we separated them into two groups for statistical comparison, one with levels lower than 6% (*mdx-Xist*$^{\Delta hs}$ < 6%; mean 3.9% ± 0.4%; n = 10) and one with levels of more than 6% (*mdx-Xist*$^{\Delta hs}$ > 6%; mean 11.0% ± 1.5%; n = 10).

### 3.1. In vivo *performance tests*

To determine the *in vivo* effects of the low dystrophin levels, mice were weighed and tested for respiratory function, inverted mesh hanging and grip-strength. *Mdx-Xist*$^{\Delta hs}$ and *mdx* mice did not differ in mean body weight, but were both ~30% heavier than the controls groups C57BL10/ScSnJ and *Xist*$^{\Delta hs}$ (i.e. the homozygous *Xist*$^{\Delta hs}$ mice, which carry a mutation in the *Xist* promoter that coordinates X-inactivation, and have 100% dystrophin) (Fig. 2A). In whole body plethysmography, the respiration amplitude (absolute as well as body weight-normalized) and rate did not differ between the mouse strains, except for the *mdx-Xist*$^{\Delta hs}$ mice, which had a somewhat lower normalized amplitude than the *Xist*$^{\Delta hs}$ control strain (Fig. 2B–D). No differences were found between *mdx-Xist*$^{\Delta hs}$ > 6% and *mdx-Xist*$^{\Delta hs}$ < 6% groups in mean body

weights or respiration parameters. In the inverted mesh hang test, 4/8 of the *mdx* mice and 7/20 of the *mdx-Xist*$^{\Delta hs}$ mice were not able to complete 240 s hanging, even with three attempts allowed (Fig. 2E). No clear difference in the performance of *mdx-Xist*$^{\Delta hs}$ > 6% and *mdx-Xist*$^{\Delta hs}$ < 6% was found; 3/10 and 4/10 mice, respectively, were not able to complete the test. The control mice all accomplished the test. Of the *mdx*$^{+/-}$ group (i.e. heterozygous *mdx* mice expressing ~50% dystrophin), only one mouse did not manage to hang the maximum time, although it hung for almost 180 s. The mean pulling force obtained in grip strength testing was equally reduced (by ~35%) in *mdx-Xist*$^{\Delta hs}$ and *mdx* mice, as compared to control and *mdx*$^{+/-}$ mice (Fig. 2F,G). Normalized to body weight, pulling force of *Xist*$^{\Delta hs}$ control mice was ~30% higher than the C57BL10/ScSnJ controls and *mdx*$^{+/-}$ mice (Fig. 2H). No difference was present between *mdx-Xist*$^{\Delta hs}$ > 6% and *mdx-Xist*$^{\Delta hs}$ < 6% groups, and there was no correlation between the dystrophin level and pulling force (Fig. 2I). During the 10 successive pulls of the grip strength test, the force of the control and *mdx*$^{+/-}$ strains remained more or less constant, whereas that of the *mdx, mdx-Xist*$^{\Delta hs}$ > 6% and *mdx-Xist*$^{\Delta hs}$ < 6% mice clearly waned in a similar fashion for both strains (Fig. 2J). Thus, the *in vivo* muscle function assessments revealed no improvements of the *mdx-Xist*$^{\Delta hs}$ mice, as compared to the *mdx* mice, while *mdx*$^{+/-}$ mice showed muscle strength comparable to that of controls.

To further assess *in vivo* muscle function and, more specifically, NMJ function, we performed 40 Hz repetitive nerve stimulation electromyography in anaesthetized mice (Fig. 3). The initial CMAP amplitude was ~40% higher in *Xist*$^{\Delta hs}$ control mice as compared to the C57BL/10ScSnJ control mice (Fig. 3A). This apparent strain difference may have contributed to the ~10%–20% larger initial CMAP amplitude of *mdx-Xist*$^{\Delta hs}$ mice (with their mixed genetic background), as compared to *mdx* mice. During 40 Hz repetitive nerve stimulation a slight CMAP decrement was seen, which showed a dystrophin level-associated trend, from being near-stable in the controls to decrementing by ~5% and ~7% in the *mdx-Xist*$^{\Delta hs}$ and *mdx* group, respectively (Fig. 3B). However, this difference was not statistically significant and when the CMAP decrement percentages of single *mdx-Xist*$^{\Delta hs}$ mice were plotted against their individual dystrophin percentages, linear regression analysis did not show a statistically significant correlation (Fig. 3C). In line with this, no differences were found between mean values of *mdx-Xist*$^{\Delta hs}$ > 6% and *mdx-Xist*$^{\Delta hs}$ < 6% groups.

### 3.2. Ex vivo *muscle contraction assessments*

Contraction force of diaphragm muscle *ex vivo* was measured upon stimulation of the phrenic nerve. Absolute twitch contraction force was rather similar across most strains (Fig. 4A). *Mdx* muscles had ~50% lower twitch force than *Xist*$^{\Delta hs}$ and *mdx-Xist*$^{\Delta hs}$ muscles, this difference being most likely due to the different genetic backgrounds, in view of the tendency for a greater twitch force in *Xist*$^{\Delta hs}$ control mice as compared to the C57BL/10ScSnJ controls. When normalized to body weight, a statistically significant decrease was apparent in *mdx* and *mdx*$^{+/-}$ muscles as compared to *Xist*$^{\Delta hs}$ muscles (Fig. 4B). Similar trends were observed with 40 Hz tetanic contraction force (Fig. 4C–D). No statistically significant differences were found for any of these contraction parameters between the mean values of *mdx-Xist*$^{\Delta hs}$ > 6% and *mdx-Xist*$^{\Delta hs}$ < 6% groups.

We also measured tetanic contraction in the presence of the reversible AChR antagonist d-tubocurarine, to assess the synaptic strength of NMJs. Tetanic contractions of *Xist*$^{\Delta hs}$ and *mdx-Xist*$^{\Delta hs}$ tended to be more reduced than that of muscles of the other groups (Fig. 4E–F). A considerable and statistically significant difference in sensitivity to d-tubocurarine was observed between muscles of *Xist*$^{\Delta hs}$ and C57BL/10ScSnJ control mice ($P < 0.05$, Fig. 4F). This control strain difference in d-tubocurarine sensitivity may explain the greater sensitivity in the muscles of *mdx-Xist*$^{\Delta hs}$ mice as compared to the muscles of C57BL/10ScSnJ controls, *mdx*$^{+/-}$ and *mdx* mice, because of the mixed genetic background of *mdx-Xist*$^{\Delta hs}$ mice. Although this somewhat complicates the interpretation of these results, it seems reasonable to conclude that *mdx-Xist*$^{\Delta hs}$ NMJs do at least not show less sensitivity to d-tubocurarine than *mdx* NMJs.

### 3.3. *Most aspects of the aberrant electrophysiology of dystrophin-deficient NMJs are not normalized by low levels of dystrophin*

Electrophysiological synaptic parameters were studied with intracellular microelectrode measurements at single NMJs of diaphragm muscle. In 1/8, 6/20 and 3/7 of the studied *mdx*$^{+/-}$, *mdx-Xist*$^{\Delta hs}$ and *mdx* diaphragms, respectively, we encountered a small amount (~2%–15%) of synaptically 'silent' NMJs, i.e. no MEPPs were present and no muscle fibre action potential occurred upon nerve stimulation (Fig. 5A). No clear difference with respect to this phenomenon was seen between the *mdx-Xist*$^{\Delta hs}$ and *mdx* groups, nor between *mdx-Xist*$^{\Delta hs}$ > 6% and *mdx-Xist*$^{\Delta hs}$ < 6% groups. In diaphragms from all the C57BL/10ScSnJ and *Xist*$^{\Delta hs}$ control mice, all muscle fibre impalements yielded synaptically active NMJs. MEPP amplitude was found decreased by ~35% in *mdx-Xist*$^{\Delta hs}$ as well as *mdx* NMJs, as compared to controls (Figs. 5B and 6). No correlation between mean MEPP amplitude and dystrophin level of individual *mdx-Xist*$^{\Delta hs}$ mice was observed (Fig. 5C). MEPP amplitudes at *mdx*$^{+/-}$ NMJs, however, equalled those of control strains NMJs. The frequency of MEPPs did not differ statistically significantly amongst the strains (Fig. 5D). The 10%–90% rise time of the MEPPs was increased by ~25% at *mdx* NMJs, as compared to C57BL/10ScSnJ control, *mdx*$^{+/-}$ as well as *mdx-Xist*$^{\Delta hs}$ NMJs (Fig. 5E). However, no correlation between mean MEPP rise time and dystrophin level of individual *mdx-Xist*$^{\Delta hs}$ mice was observed (Fig. 5F). Mean *mdx-Xist*$^{\Delta hs}$ MEPP rise time was similar to the *Xist*$^{\Delta hs}$ controls. Amongst the different strains there was no difference in the mean intra-NMJ variation coefficient (VC) of the MEPP amplitude (Fig. 5G). Inter-NMJ VC of the mean MEPP amplitude within muscles was increased in *mdx-Xist*$^{\Delta hs}$ and *mdx* mice, as compared to C57BL/10ScSnJ control muscles (Fig. 5H). None of the mean values of these MEPP parameters differed statistically significantly between *mdx-Xist*$^{\Delta hs}$ > 6% and *mdx-Xist*$^{\Delta hs}$ < 6% groups. It can be concluded that the low levels of dystrophin in *mdx-Xist*$^{\Delta hs}$

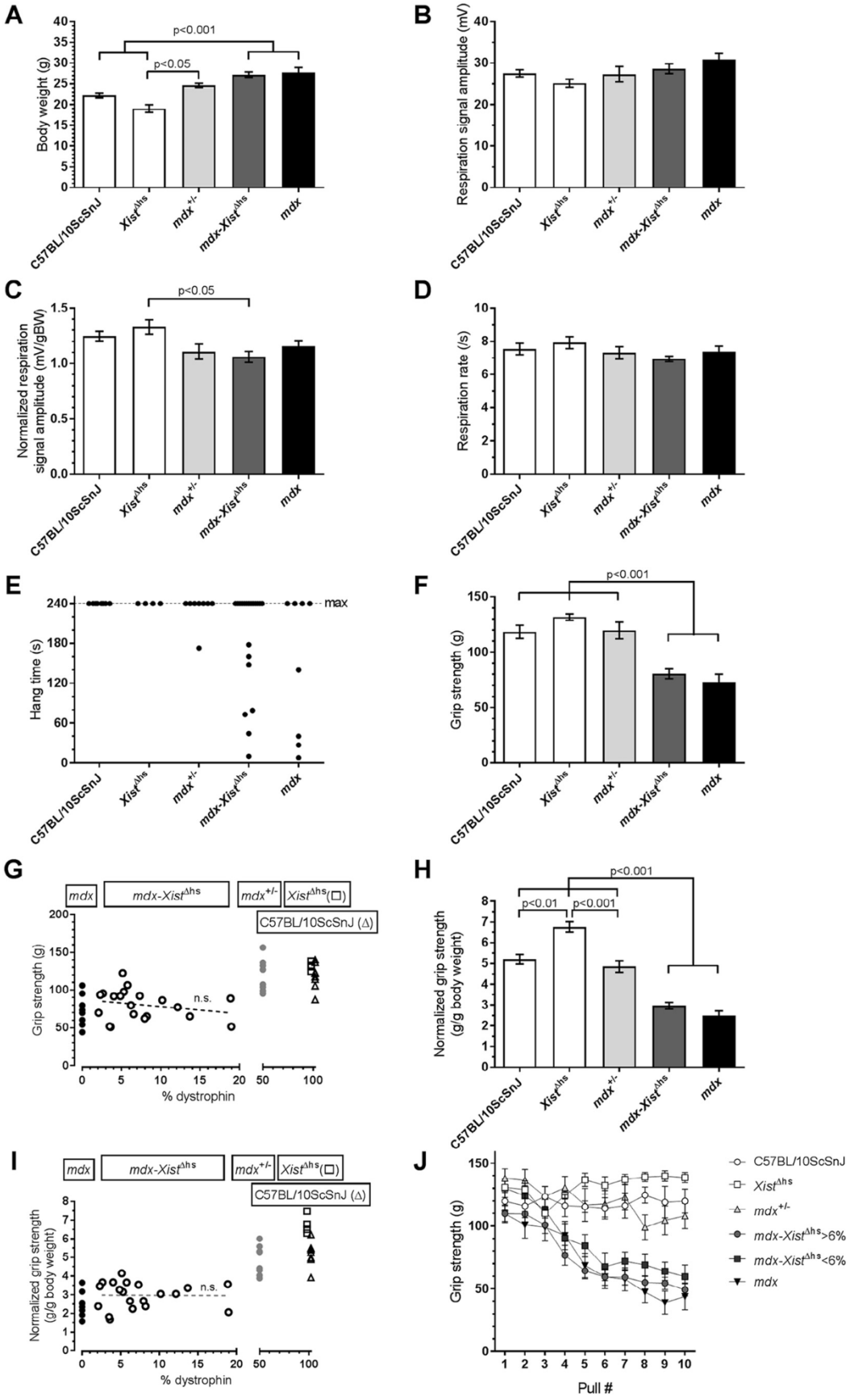
A
Body weight (g)
p<0.001
p<0.05
C57BL/10ScSnJ
Xist^Δhs
mdx^+/-
mdx-Xist^Δhs
mdx
B
Respiration signal amplitude (mV)
C
Normalized respiration signal amplitude (mV/gBW)
p<0.05
D
Respiration rate (/s)
E
Hang time (s)
max
F
Grip strength (g)
p<0.001
G
mdx
mdx-Xist^Δhs
mdx^+/-
Xist^Δhs(□)
C57BL/10ScSnJ (△)
Grip strength (g)
n.s.
% dystrophin
H
Normalized grip strength (g/g body weight)
p<0.001
p<0.01
p<0.001
I
mdx
mdx-Xist^Δhs
mdx^+/-
Xist^Δhs(□)
C57BL/10ScSnJ (△)
Normalized grip strength (g/g body weight)
n.s.
% dystrophin
J
Grip strength (g)
Pull #
C57BL/10ScSnJ
Xist^Δhs
mdx^+/-
mdx-Xist^Δhs>6%
mdx-Xist^Δhs<6%
mdx

Fig. 2. *In vivo* neuromuscular performance tests. (A) Body weight was increased in *mdx-Xist*$^{\Delta hs}$ and *mdx* mice compared to the controls. (B) No differences in whole-body plethysmography signal amplitude. (C) Respiration amplitude normalized to body weight. (D) Respiration rate did not differ amongst the mouse models. (E) In the inverted mesh hang test, 7 of the 20 *mdx-Xist*$^{\Delta hs}$ mice and 4 of the 8 *mdx* mice were not able to hang for 240 s. (F) Grip strength in both *mdx-Xist*$^{\Delta hs}$ and *mdx* mice was ~40% less than in control and *mdx*$^{+/-}$ mice. (G) There was no correlation between the grip strength and dystrophin percentage of individual *mdx-Xist*$^{\Delta hs}$ mice. (H–I) Similarly, no correlation was found when the grip strength values were normalized for body weight. (J) Pulling force during the 10 successive trials of the grip strength test declined in *mdx-Xist*$^{\Delta hs}$ and *mdx* mice whereas that of *mdx*$^{+/-}$ and wild-type mice remained constant. No difference was found between the groups of *mdx-Xist*$^{\Delta hs}$ mice with dystrophin levels of either >6% or <6%. N = 4–20 mice per genotype group, aged 2–5 months. Error bars represent S.E.M. In (G) and (H) the *Xist*$^{\Delta hs}$ control mice are indicated with an open square and the C57BL/10ScSnJ control mice with an open triangle. n.s. = not statistically significant.

mice do not correct the reductions in MEPP amplitude as present in *mdx* NMJs, while 50% dystrophin in the *mdx*$^{+/-}$ mice does. On the other hand, elevated MEPP rise time seems to be normalized by low levels of dystrophin.

The amplitudes of EPPs, evoked by 0.3 Hz nerve stimulation, were slightly smaller (~10%) in both *mdx-Xist*$^{\Delta hs}$ and *mdx* NMJs (Fig. 6, 7A). This was only statistically significant in comparison to the *mdx*$^{+/-}$ group. The 10%–90% rise time of these EPPs in *mdx* NMJs was ~25% increased as compared to the C57BL/10ScSnJ control and *mdx*$^{+/-}$ NMJs (Fig. 7B). Half-width of the EPPs was increased by ~15% in *mdx-Xist*$^{\Delta hs}$ and *mdx* mice compared to C57BL/10ScSnJ. In addition, the half-width of EPPs in *mdx* NMJs was also increased compared to *Xist*$^{\Delta hs}$ and *mdx*$^{+/-}$ NMJs (Fig. 7C). Furthermore, the EPP decay time was increased by ~30% in the *mdx-Xist*$^{\Delta hs}$ and *mdx* NMJs, compared with C57BL/10ScSnJ control. The *Xist*$^{\Delta hs}$ control differed only from the *mdx* mice (Fig. 7D). The half-width and decay time of EPPs of *mdx-Xist*$^{\Delta hs}$ mice tended to be somewhat smaller than those of the *mdx* mice, but this was not statistically significant. The quantal content, i.e. the number of ACh quanta released per nerve impulse at 0.3 Hz stimulation, was clearly increased (by ~35%) at NMJs of both *mdx-Xist*$^{\Delta hs}$ and *mdx* mice compared to the controls, as well as to *mdx*$^{+/-}$ NMJs (Fig. 7E). Although no statistically significant differences were seen between mean quantal contents of the *mdx-Xist*$^{\Delta hs}$ and *mdx* groups, nor between those of the *mdx-Xist*$^{\Delta hs}$ > 6% and *mdx-Xist*$^{\Delta hs}$ < 6% groups, a weak but statistically significant inverse correlation was observed between mean quantal content and the dystrophin level of individual *mdx-Xist*$^{\Delta hs}$ mice (Fig. 7F).

At high-rate (40 Hz) nerve stimulation, successive EPPs in normal NMJs run down to a steady level of ~80% of the initial amplitude. This is due to rate-limiting factors in the ACh release mechanism. At NMJs of both *mdx-Xist*$^{\Delta hs}$ and *mdx* mice the EPP rundown was more pronounced than in controls, i.e. to a more or less similar level of ~75% of the first EPP (Fig. 7G–H). No correlation was seen between mean EPP rundown and dystrophin percentage of individual *mdx-Xist*$^{\Delta hs}$ mice (not shown). The EPP rundown level of *mdx*$^{+/-}$ NMJs did not differ from the controls.

Thus, the low levels of dystrophin in *mdx-Xist*$^{\Delta hs}$ mice did not normalize most electrophysiological aberrations of ACh release in dystrophin-deficient NMJs in *mdx* mice, although there was a tendency for normalization of the slower MEPP and EPP kinetics. In addition, quantal content was weakly inversely correlated with dystrophin level. *Mdx*$^{+/-}$ NMJs showed no deficits in synaptic electrophysiology; apparently the ~50% dystrophin level is sufficient for normal NMJ function.

### 3.4. AChR cluster fragmentation is retained in low level dystrophin NMJs

In a proportion of the functionally studied mice, AChR geometry and dystrophin localization at NMJs was studied with (immuno-)fluorescence confocal laser-scanning microscopy. Clear AChR cluster fragmentation was present in *mdx* as well as in *mdx-Xist*$^{\Delta hs}$ NMJs (Fig. 8A). The amount of separate AChR clusters at diaphragm NMJs was clearly higher (~6 islets per NMJ) in *mdx* NMJs, as compared to the C57BL/10ScSnJ and *Xist*$^{\Delta hs}$ controls (both only ~2 islets per NMJ) (Fig. 8B). The mean AChR islet number in NMJs of *mdx-Xist*$^{\Delta hs}$ mice was somewhat lower than in *mdx* (~5 per NMJ), but this difference was not statistically significant. No difference was observed between *mdx-Xist*$^{\Delta hs}$ > 6% and *mdx-Xist*$^{\Delta hs}$ < 6% mice. The total AChR area per NMJs in the diaphragm was ~250–300 μm$^2$ and did not differ statistically significantly amongst the different genotype groups (Fig. 8C). A proportion of the *mdx-Xist*$^{\Delta hs}$ NMJs had control-like NMJ appearance, i.e. only a few AChR islets and a more or less intact pretzel-shaped structure. Such NMJs were encountered in any area within the muscle, with no apparent grouped localization.

High-magnification immunofluorescence confocal laser-scanning microscopy of *mdx-Xist*$^{\Delta hs}$ ETA muscles revealed variable, but generally low-intense dystrophin staining at most NMJs, which roughly but certainly not exactly co-localized with the area stained for AChR with fluorescently labelled α-BTx (Fig. 9A). *Mdx*$^{+/-}$ NMJs had a similar AChR and dystrophin morphological appearance as C57BL/10ScSnJ and *Xist*$^{\Delta hs}$ controls, while *mdx* NMJs clearly showed AChR cluster fragmentation and absence of dystrophin (Fig. 9B).

## 4. Discussion

With therapies emerging that aim to restore dystrophin protein in muscles to treat or slow down DMD [31,32], it is important to know the rescuing effects of low percentages dystrophin protein on all different components of the muscle. This includes the effects on functional and morphological aberrations at the dystrophic NMJ, such as reduced safety factor of neuromuscular transmission and AChR cluster fragmentation, demonstrated by us previously in DMD mouse models [5]. Here we show in mice expressing only ~2%–19% of normal dystrophin in their diaphragm, that there is virtually no normalization of the deficits in synaptic signalling and morphology of the NMJ. We also demonstrate that NMJ function and morphology of *mdx*$^{+/-}$ mice, expressing ~50% of normal dystrophin, is near-normal. Thus, our study shows that presence of less than ~19% of the normal level of dystrophin

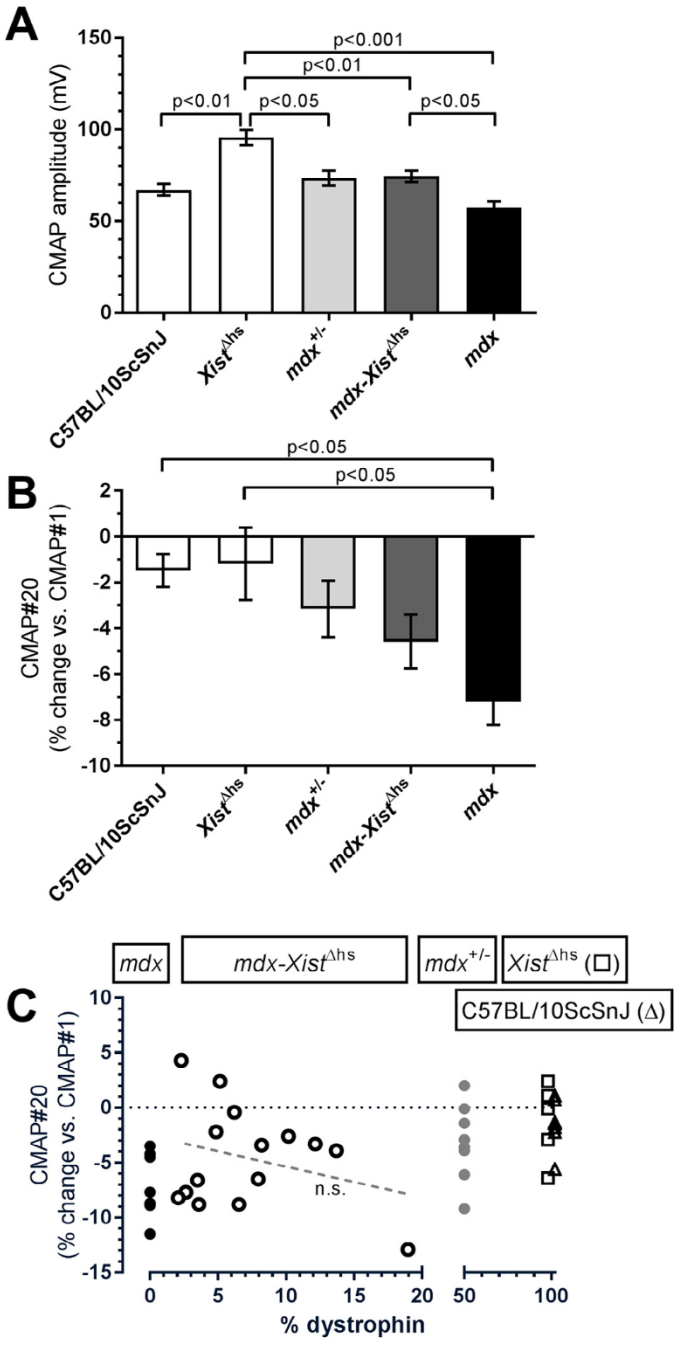


Fig. 3. Repetitive nerve stimulation electromyography. Compound muscle action potentials (CMAPs) were recorded from the calf muscles of anaesthetized mice during 40 Hz supramaximal sciatic nerve stimulation. (A) The amplitude of the first CMAP of the train in *Xist*$^{\Delta hs}$ control mice was ~35% higher than that of the C57BL/10ScSnJ controls. This genetic background difference possibly explains the somewhat larger first CMAP in *mdx-Xist*$^{\Delta hs}$ mice, as compared to *mdx*. (B) CMAP decrement was present in the *mdx* mice and did not differ statistically significantly from that of *mdx-Xist*$^{\Delta hs}$ mice. (C) No correlation was present between CMAP decrement and dystrophin percentage in the *mdx-Xist*$^{\Delta hs}$ mice. N = 5–20 mice per genotype group, aged 2–5 months. Columns in (A) and (B) represent group means, error bars represent S.E.M. Symbols in (C) are values of the individual mice; *Xist*$^{\Delta hs}$ control mice are indicated with open squares and the C57BL/10ScSnJ control mice with open triangles. n.s. = not statistically significant.

protein is insufficient to normalize the NMJ deficits of *mdx* mice, but that ~50% of normal dystrophin level seems to be enough for normal synaptic function of the NMJ.

Dystrophin levels of the diaphragm muscle of the *mdx-Xist*$^{\Delta hs}$ mice investigated here varied between ~2% and 19% of normal, with a group mean of 7.5%. In a previously reported series of 24 female *mdx-Xist*$^{\Delta hs}$ mice (with *mdx* and *Xist*$^{\Delta hs}$ parents originating from the same breeding colonies as used in the current study), a wider range of dystrophin percentages was found of 3%–47% of normal, and a higher group mean of 22.7% [25]. Dystrophin levels in that study were determined in quadriceps muscle, which was shown in a sample of 6 *mdx-Xist*$^{\Delta hs}$ mice in the same study to express an average of ~50% more dystrophin than the diaphragm muscle of those mice. However, this explains only a part of the much lower range and mean of dystrophin protein levels observed in the current series. Apparently, series variation exists due to (subtle) differences in the skewedness of X chromosomal silencing in the *mdx-Xist*$^{\Delta hs}$ model. Perhaps, litter dependent effects are also involved.

*In vivo* strength and endurance tests showed muscle weakness in *mdx* mice, as compared to the control strains. Although there were slight tendencies of improvement, no statistically significant changes were observed for the *mdx-Xist*$^{\Delta hs}$ mice as compared to *mdx*, and no positive correlation was seen in linear regression when the grip strength of individual mice was plotted against their dystrophin level. The subtle improvements as compared to *mdx* may even have resulted from the mixed genetic background of *mdx-Xist*$^{\Delta hs}$ mice, which is the inherent result of *mdx-Xist*$^{\Delta hs}$ mice being produced by mating of *Xist*$^{\Delta hs}$ females, which have a C57BL/6 X CBA background [26], and male *mdx* mice which have a C57BL/10ScSnJ background. For completeness, we included females of both these control strains in our studies. We observed that they were similar for most of the *in vivo* parameters but differed to quite some extent in the body weight-normalized grip strength parameter, *Xist*$^{\Delta hs}$ mice being ~30% stronger than C57BL/10ScSnJ mice. Thus, this genetic background difference may have accounted for the observed improvement tendencies in *mdx-Xist*$^{\Delta hs}$ mice, as compared to the *mdx* mice, which have a pure C57BL/10ScSnJ genetic background. The lack of clear muscle strength improvement in *mdx-Xist*$^{\Delta hs}$ mice seems to differ from an earlier study which reported strength increases in *mdx-Xist*$^{\Delta hs}$ mice, even with dystrophin percentages in the lowest category (<15%), as assessed in quadriceps muscle and thus with diaphragm dystrophin percentages probably in the range of the current series [25]. Furthermore, *mdx*$^{3cv}$ mice expressing ~5% dystrophin, as assessed in tibialis anterior, have been shown to have more muscle strength than *mdx*$^{4cv}$ mice, which have no dystrophin at all [24]. In addition, ~ 5% dystrophin expressed in an *mdx*$^{3cv}$/*utrn*$^{-/-}$ compound mutant strain drastically improved the phenotype, as compared to *mdx*/*utrn*$^{-/-}$ mice without dystrophin [33]. Similarly, *mdx*/*utrn*$^{-/-}$-*Xist*$^{\Delta hs}$ mice with percentages of dystrophin below 4% clearly improved [34]. The reasons for the apparent discrepancies with the current set of *mdx-Xist*$^{\Delta hs}$ mice remain unclear.

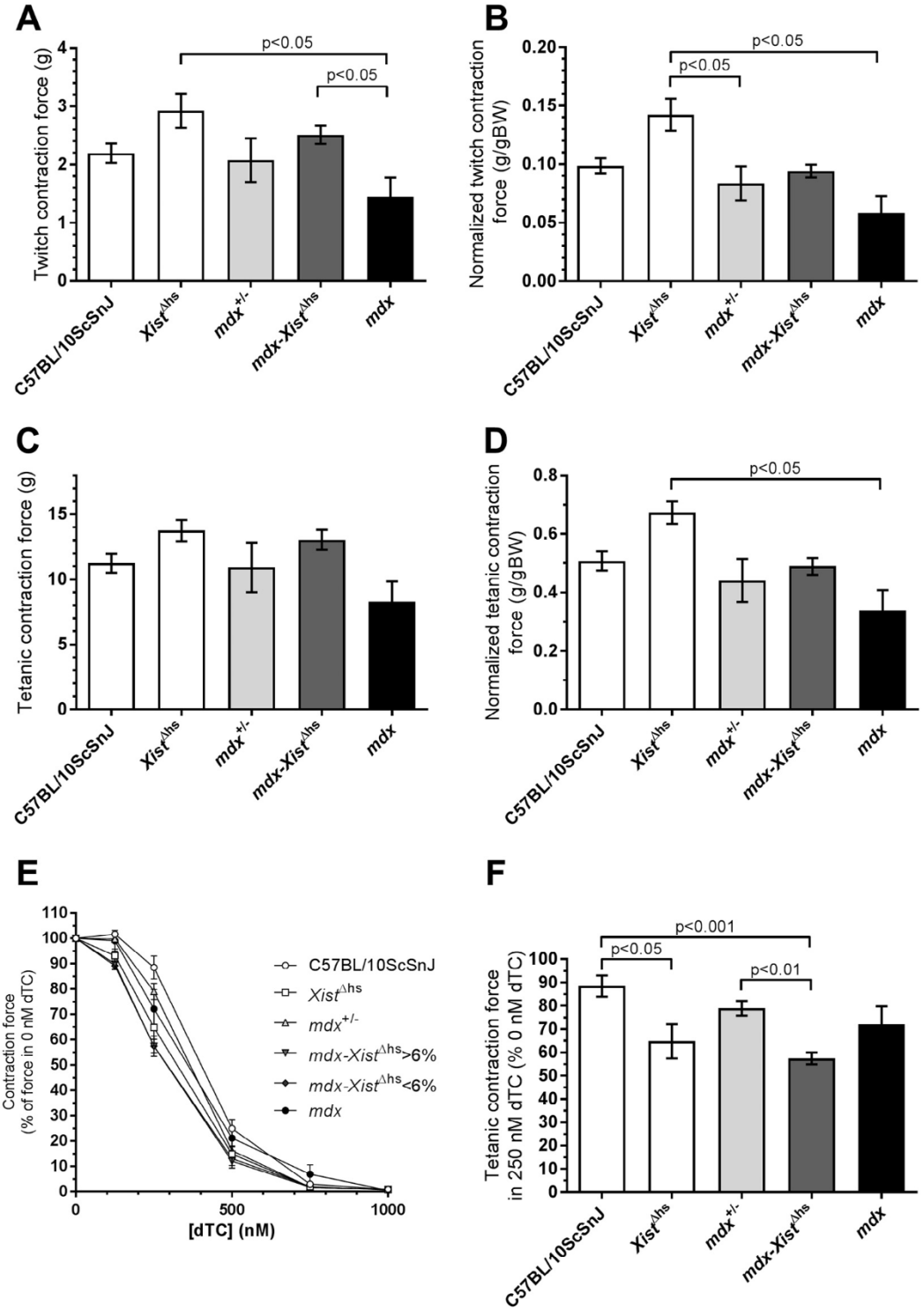


Fig. 4. *Ex vivo* diaphragm muscle contraction measurements. Supramaximal stimulation of the phrenic nerve. (A) Absolute twitch contraction force. (B) Twitch contraction force normalized for body weight. (C) Tetanic contraction force determined at 2 s after start of the 40 Hz nerve stimulation. (D) Tetanic contraction force normalized for body weight. (E) Concentration-effect relationship between tetanic contraction and the reversible AChR antagonist d-tubocurarine (dTC). (F) Tetanic contraction force in the presence of 250 nm dTC as percentage of the contraction force without dTC. Under this condition, the relative contraction force in *Xist*$^{\Delta hs}$ control mice was ~35% smaller than that of the C57BL/10ScSnJ controls. This genetic background difference possibly explains the (not statistically significant) tendency of a smaller relative contraction force of *mdx-Xist*$^{\Delta hs}$ diaphragms, as compared to *mdx* and *mdx*$^{+/-}$ mice. N = 3–18 mice per genotype group, aged 2–5 months. Bars represent mean ± SEM.

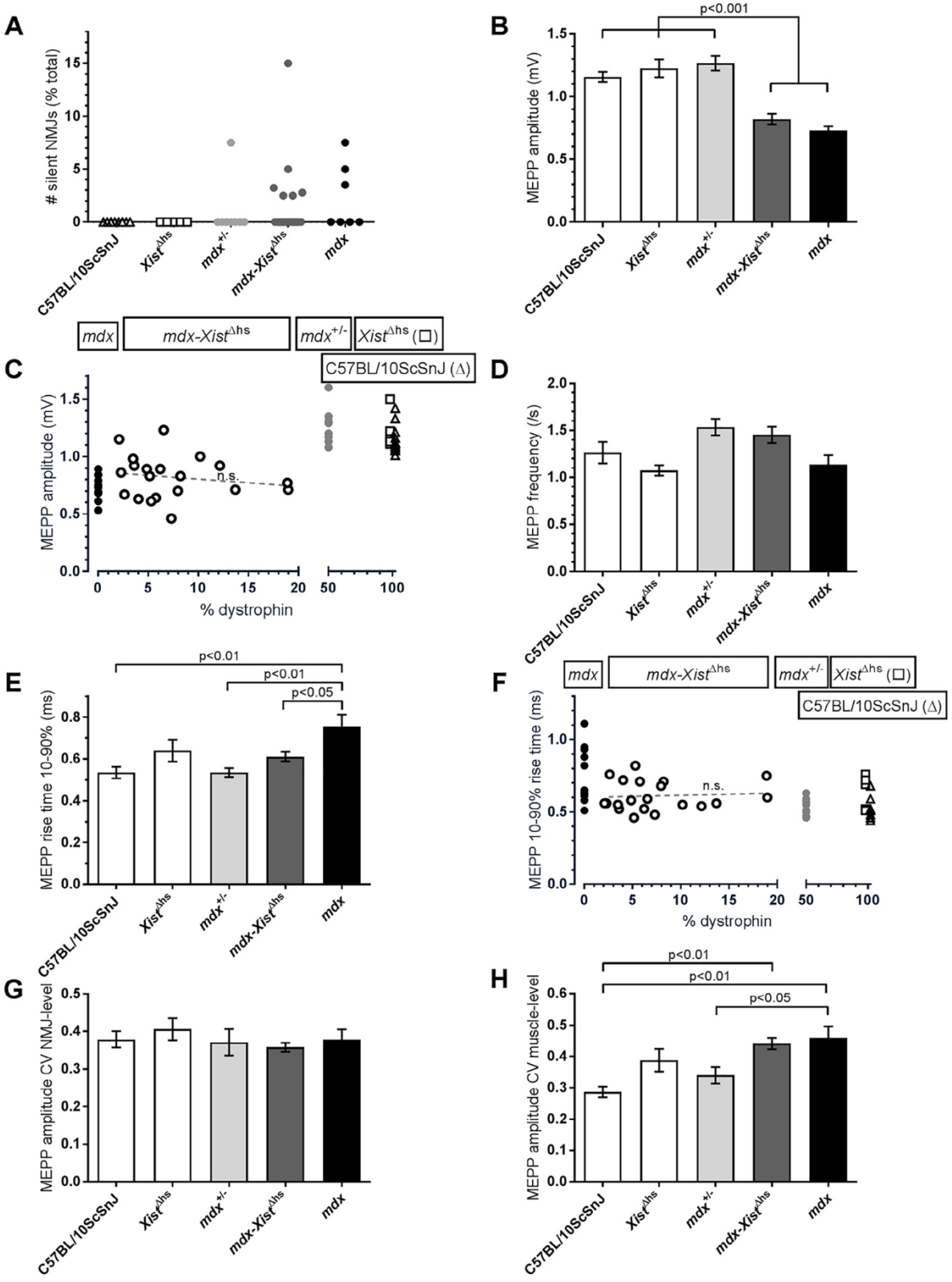


Fig. 5. Electrophysiological analyses of miniature endplate potentials (MEPPs) at neuromuscular junctions (NMJs). (A) About half of the *mdx-Xist*$^{\Delta hs}$ and *mdx* mice showed some degree of synaptically silent NMJs in their diaphragm. (B) Similar extent of MEPP amplitude reduction at *mdx-Xist*$^{\Delta hs}$ and *mdx* NMJs. (C) No correlation was present between MEPP amplitude and dystrophin percentage in the *mdx-Xist*$^{\Delta hs}$ mice. (D) MEPP frequency did not differ amongst the mouse models. (E) The relatively slow 10%–90% rise time of MEPPs at *mdx* NMJs was normalized at *mdx-Xist*$^{\Delta hs}$ NMJs. (F) No correlation was present between the 10%–90% rise time and dystrophin percentage in the *mdx-Xist*$^{\Delta hs}$ mice. (G) Intra-NMJ amplitude variability (coefficient of variation, CV) of the MEPPs did not differ amongst the mouse models. (H) Inter-NMJ variation of MEPP amplitude within muscles was somewhat higher in *mdx-Xist*$^{\Delta hs}$ and *mdx mice*. N = 4–20 mice per genotype group, aged 2–5 months. Error bars represent S.E.M. In (C) and (F), the *Xist*$^{\Delta hs}$ control mice values are indicated with open squares and the C57BL/10ScSnJ control mice values with open triangles. n.s. = not statistically significant.

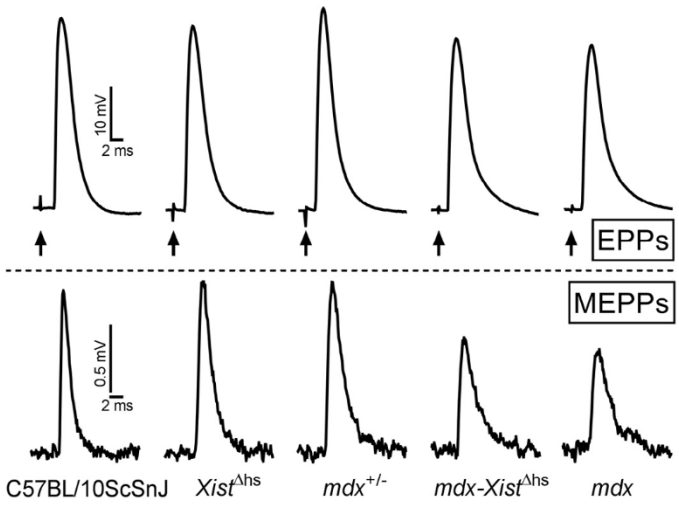


Fig. 6. Representative examples of EPPs and MEPPs recorded in the different genotype groups. Upper panel shows examples of EPPs recorded at diaphragm NMJs, with the moment of phrenic nerve stimulation indicated by arrows. Lower panel shows examples of MEPPs.

*In vivo* repetitive nerve stimulation electromyography showed that *mdx-Xist*$^{\Delta hs}$ mice had a somewhat larger first CMAP than *mdx* mice. However, this was probably due to the mixed genetic background of *mdx-Xist*$^{\Delta hs}$ mice, because the first CMAP of *Xist*$^{\Delta hs}$ control mice was found to be ~40% larger than that of C57BL/10ScSnJ control mice, the latter forming the genetic background of *mdx* mice. A normal initial CMAP amplitude was observed by us in the *mdx*$^{+/-}$ mice, when compared to the matching C57BL/10ScSnJ control. The decrement of CMAPs during the repetitive nerve stimulation in both the C57BL/10ScSnJ and *Xist*$^{\Delta hs}$ control strains was negligible, indicating sustained synaptic transmission of NMJs. In the *mdx*$^{+/-}$, *mdx-Xist*$^{\Delta hs}$ and *mdx* mice a trend of an increasing extent of CMAP decrement was found, statistically significant only for the *mdx* group, which had ~7% decrement. This suggests mild NMJ dysfunction resulting in use-dependent block in a proportion of NMJs during intense activity. Apparently, the levels of dystrophin in the investigated *mdx-Xist*$^{\Delta hs}$ mice were still too low to normalize NMJ function and rescue CMAP decrement. The ~50% dystrophin in *mdx*$^{+/-}$ mice, however, almost normalized CMAP decrement. While several clinical electromyographical studies in female DMD carriers have demonstrated myopathic features [20,35,36], to our knowledge no human electromyography data is published on CMAP decrement upon repetitive nerve stimulation.

As stated above, dystrophin levels in limb muscles of *mdx-Xist*$^{\Delta hs}$ mice are most likely ~50% higher than in diaphragm [25]. We have no indication that the dystrophin levels of limb and diaphragm muscles would not be correlated in individual mice. Therefore, although the exact percentage value as determined in diaphragm muscle might not apply to the muscles responsible for performance in the grip strength test, inverted mesh test and electromyography, the inter-mouse dystrophin level variation pattern was likely similar to that established from diaphragm dystrophin level analysis.

Our *ex vivo* microelectrode studies of synaptic signals at the NMJ showed that the low dystrophin levels of the *mdx-Xist*$^{\Delta hs}$ mice did not restore the aberrant electrophysiological parameters of *mdx* NMJs to normal values, while the ~50% of *mdx*$^{+/-}$ did. The MEPP amplitudes of *mdx-Xist*$^{\Delta hs}$ NMJs were comparable to those in *mdx* NMJs, i.e. both were ~35% smaller than at NMJs of the control strains. Similarly, the other distinct electrophysiological features of *mdx* NMJs (i.e. increased quantal content and a more pronounced rundown of EPPs during intense synaptic activity, as discussed in our previous work [5]), were not normalized in the *mdx-Xist*$^{\Delta hs}$ NMJs. The results of the *ex vivo* contraction experiments assessing the d-tubocurarine sensitivity of NMJ transmission are in line with these observations.

EPPs and MEPPs of *mdx* NMJs have slower kinetics, i.e. slower rise times, and prolonged half-widths and decay times [5]. This suggests an influence of dystrophin on AChR ion channel kinetics or other factors that influence the (M)EPP time course such as e.g. acetylcholinesterase activity or the electrical capacitance of the sarcolemma. These kinetics abnormalities tended to be normalized in the *mdx-Xist*$^{\Delta hs}$ NMJs, although statistical significance was not reached for all parameters. This may indicate that one of the first effects of increasing the level of dystrophin at the NMJ would be a normalization of the slower kinetics of the synaptic signals. However, all other parameters were not yet normalized, even not in the two *mdx-Xist*$^{\Delta hs}$ mice with dystrophin levels of ~19%, i.e. the upper end of the dystrophin spectrum of the investigated series of 20 *mdx-Xist*$^{\Delta hs}$ mice. Additional normalization of the reduced postsynaptic ACh sensitivity seems to be only possible when dystrophin is expressed at levels (much) higher than 19%.

Similarly, the postsynaptic morphological deviations of dystrophin-deficient NMJs, i.e. the fragmented AChR clusters, were on average not normalized. However, a small minority of the *mdx-Xist*$^{\Delta hs}$ diaphragm NMJs had control-like AChR cluster appearance, i.e. a pretzel-shaped geometry with only few separate islets. In further studies, it would be interesting to specifically measure the synaptic signals at such NMJs to see if the morphological normalization is associated with normalized electrophysiology.

Each mouse skeletal muscle fibre possesses one hundred to a few hundreds of nuclei which are regularly spaced over the whole fibre with ~30 μm internuclear distance. An exception is present at the postsynaptic membrane of the NMJ, where a subsynaptic cluster of an average four nuclei exists with only 11–14 μm internuclear distance [37]. Nuclei in *mdx-Xist*$^{\Delta hs}$ muscle fibres express dystrophin mRNA at either wild-type level or not at all, leading to a patchy dystrophin presence along the sarcolemma [25]. However, at their NMJs (if they expressed dystrophin at all) such a patchy occurrence of dystrophin was not observed in the current immunohistological NMJ investigations. Most likely this is the case because if one or more of the subsynaptic nuclei express dystrophin mRNA, there will be already a quite high local protein production directly in the vicinity of the postsynaptic membrane. This may be sufficient to cause evenly distributed dystrophin protein expression in large part or even the entire postsynaptic area. The

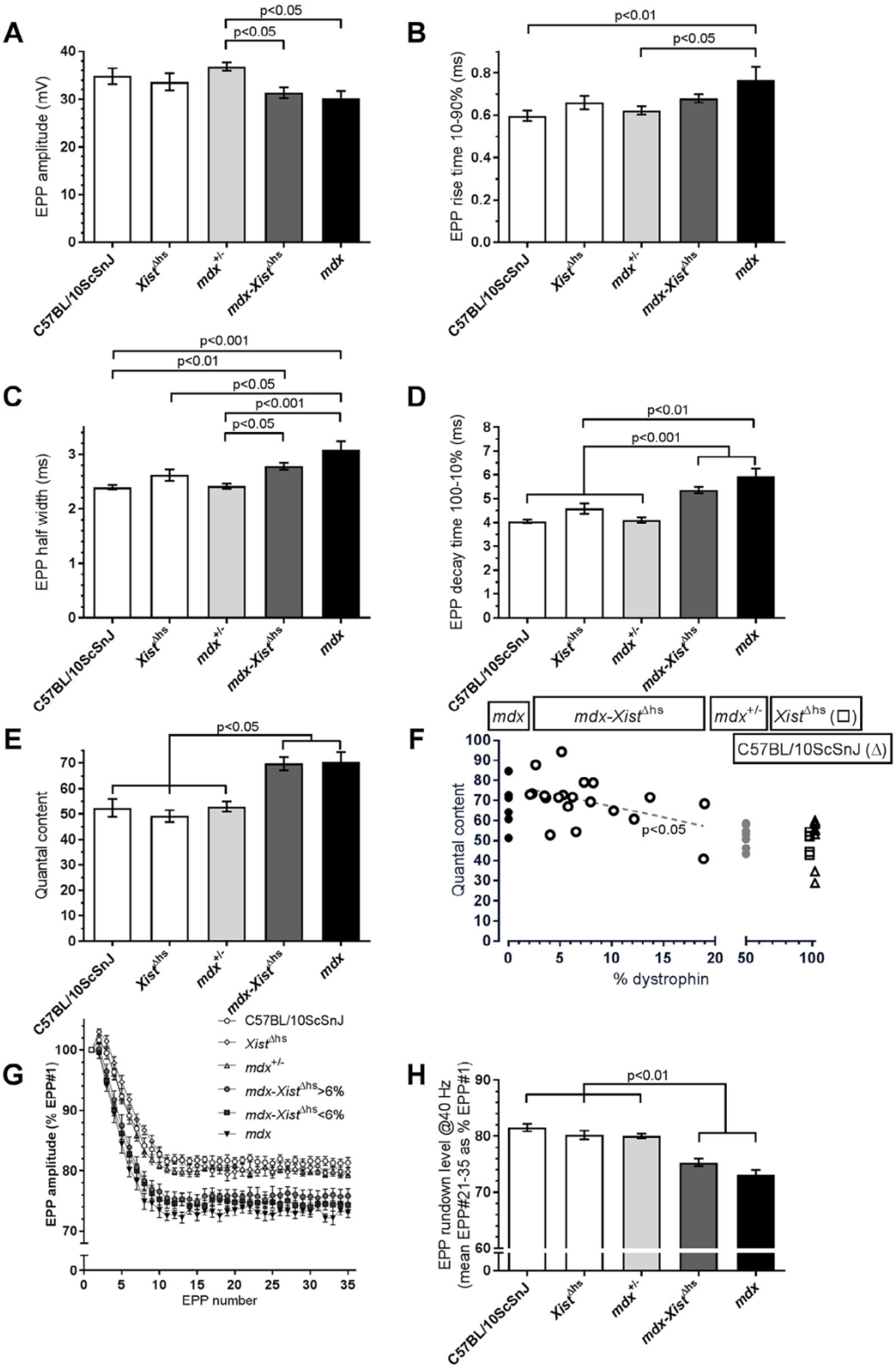


Fig. 7. Nerve stimulation-evoked ACh release is increased to a similar extent at *mdx-Xist*$^{\Delta hs}$ and *mdx* neuromuscular junctions. EPPs and MEPPs were recorded at NMJs of diaphragm-phrenic nerve preparations. (A) EPP amplitudes during 0.3 Hz nerve stimulation at *mdx-Xist*$^{\Delta hs}$ and *mdx* NMJs were not different from controls, but the EPPs at *mdx*$^{+/-}$ NMJs were slightly larger. (B) The 10%–90% rise time of *mdx* EPPs was slightly increased. (C) Half-widths of *mdx-Xist*$^{\Delta hs}$ and *mdx* EPPs were slightly increased. (D) Decay times of both *mdx-Xist*$^{\Delta hs}$ and *mdx* EPPs were increased as compared to controls. (E) The quantal content (i.e. number of ACh quanta released per nerve impulse) at 0.3 Hz stimulation was increased, as compared to controls, to a similar extent of ~35% at *mdx-Xist*$^{\Delta hs}$ and *mdx* NMJs. (F) A weak inverse correlation was observed between the mean quantal content and the dystrophin percentage of individual *mdx-Xist*$^{\Delta hs}$ diaphragms. (G) The rundown of the EPP amplitude during a 40 Hz nerve stimulation train was more pronounced at *mdx-Xist*$^{\Delta hs}$ and *mdx* NMJ, as compared to controls and *mdx*$^{+/-}$ NMJs. (H) Mean plateau level of the 21$^{st}$-35$^{th}$ EPP expressed as percentage of the first EPP. N = 5–20 mice per genotype group, aged 2–5 months. Error bars represent S.E.M. In (F), the *Xist*$^{\Delta hs}$ control mice values are indicated with open squares and the C57BL/10ScSnJ control mice values with open triangles.

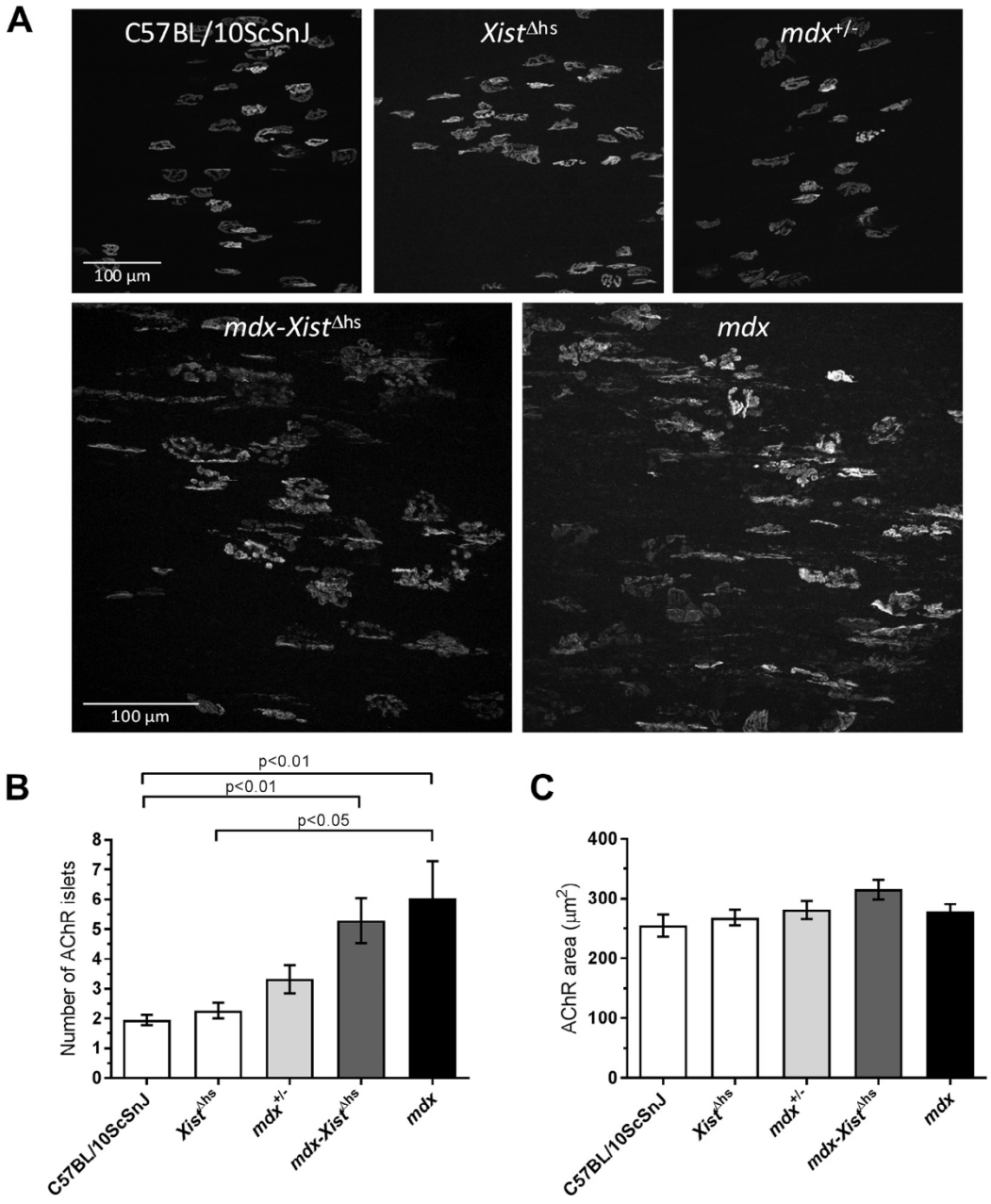


Fig. 8. The fragmentation of ACh receptor clusters at *mdx* neuromuscular junctions is not normalized at *mdx-Xist*$^{\Delta hs}$ NMJs. Confocal laser scanning fluorescence microscopy of diaphragm NMJs stained for AChRs with AlexaFluor488 labelled α-bungarotoxin. (A–B) Similar extent of increased fragmentation of AChR clusters at *mdx-Xist*$^{\Delta hs}$ and *mdx* NMJs, as compared to controls. The example picture in (A) was taken from an *mdx-Xist*$^{\Delta hs}$ mouse diaphragm expressing 2.6% dystrophin. (C) No change in total AChR staining area per NMJ between the genotypes was observed. N = 3–9 mice per genotype group, aged 2–5 months. Error bars represent S.E.M.

patchy nature of low dystrophin expression in the *mdx-Xist*$^{\Delta hs}$ model somewhat complicates the conclusion on the exact minimal level of dystrophin required to normalize NMJ function. Using interventions which induce a more uniform (and low) expression of a certain level of dystrophin (e.g. exon skipping), the minimally required percentage for NMJ normalization might be different from the current model.

## 5. Conclusions

In the current study, most of the reported electrophysiological and morphological aberrations of NMJs of *mdx* mice were also seen at NMJs of a series of 20 *mdx-Xist*$^{\Delta hs}$ mice with dystrophin levels between 2% and 19% of normal. On the other hand, the NMJ characteristics of *mdx*$^{+/-}$ mice were comparable to those of the control mouse strains. Thus, the threshold level of dystrophin for guaranteeing normal NMJ function and morphology lies somewhere between 19% and 50% of normal. Correction of the slower MEPP and EPP kinetics may already commence at lower levels. Extended studies in larger groups of *mdx-Xist*$^{\Delta hs}$ mice, with more variation and higher maximal dystrophin levels, could reveal a more precise threshold level for normal NMJ features.

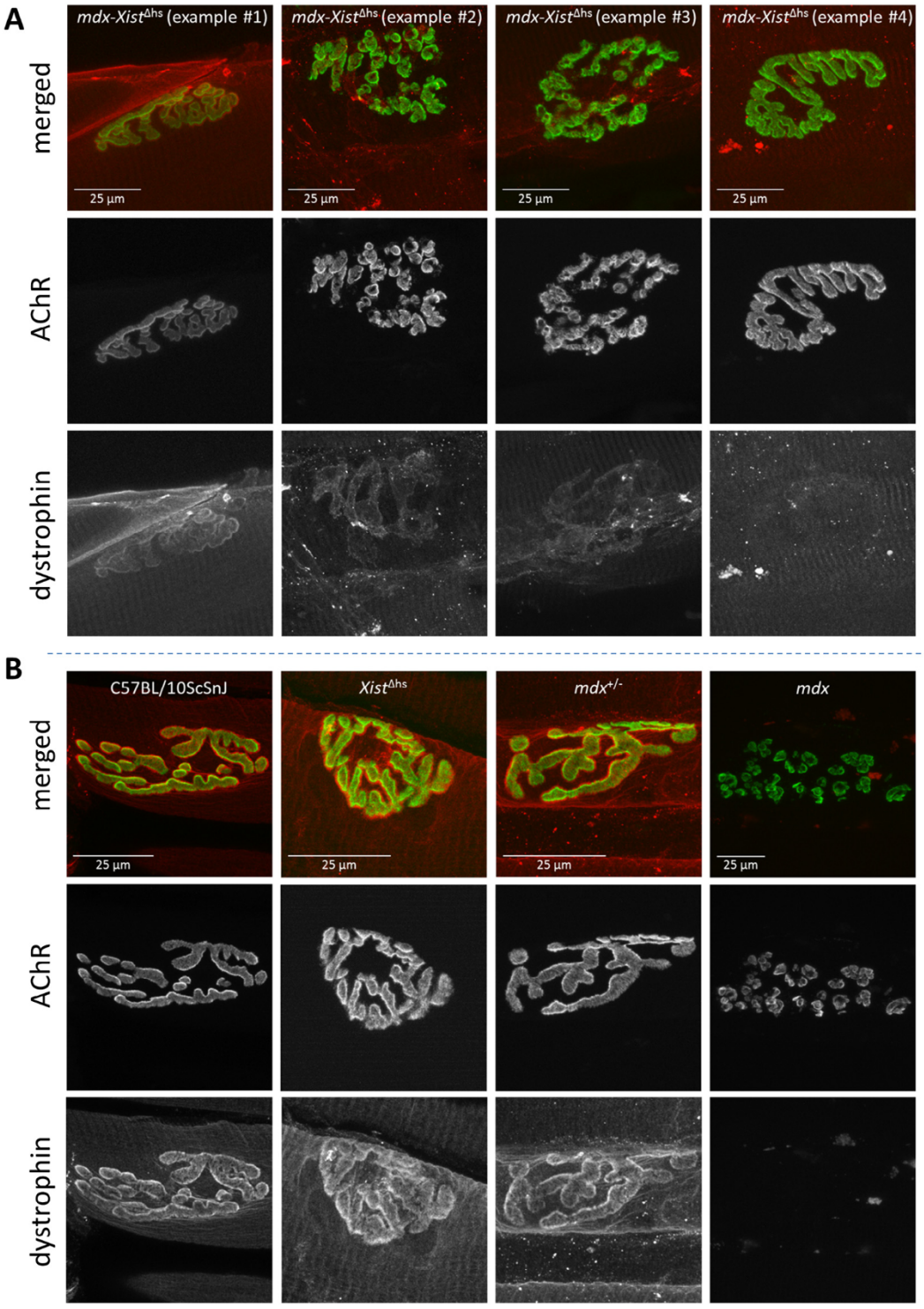


Fig. 9. Detailed laser-scanning confocal microscopy of AChR and dystrophin stainings at neuromuscular junctions. Examples of AF488-α-bungarotoxin staining of AChRs and immunostaining of dystrophin at NMJs of ETA muscles of the different genotype groups. (A) Four examples of morphological NMJ variability encountered within and between the *mdx-Xist*$^{\Delta hs}$ mouse muscles. Most NMJs in the *mdx-Xist*$^{\Delta hs}$ muscles had an *mdx*-like appearance such as those shown in examples #2 and #3. The (near-)normal AChR area profiles such as those in examples #1 and #4 were only seen in a minority of NMJs. (B) Examples of AChR and dystrophin staining at NMJs of C57BL/10ScSnJ and *Xist*$^{\Delta hs}$ control mice, as well as at NMJs of *mdx*$^{+/-}$ and *mdx* mice. Note the absence of dystrophin and evident AChR cluster fragmentation at the *mdx* example NMJ. In the merged pictures, green is the AChR staining and red the dystrophin staining.

## Funding

This work was supported by the 'Prinses Beatrix Spierfonds' (grant number W.OR11-11), 'Stichting Spieren voor Spieren', 'L'Association Française contre les myopathies' (grant numbers #15042, #16686) and the Dutch Duchenne Parent Project.

## Acknowledgments

We thank the technicians of the Microscopy Facility of the Molecular Cell Biology Department of the LUMC for excellent help with laser scanning confocal microscopy.

## References

[1] Hoffman EP, Brown RH Jr, Kunkel LM. Dystrophin: the protein product of the Duchenne muscular dystrophy locus. Cell 1987;51:919–28.
[2] Blake DJ, Weir A, Newey SE, Davies KE. Function and genetics of dystrophin and dystrophin-related proteins in muscle. Physiol Rev 2002;82:291–329.
[3] Bewick GS, Nicholson LV, Young C, O'Donnell E, Slater CR. Different distributions of dystrophin and related proteins at nerve-muscle junctions. Neuroreport 1992;3:857–60.
[4] Carlson CG, Roshek DM. Adult dystrophic (mdx) endplates exhibit reduced quantal size and enhanced quantal variation. Pflugers Arch 2001;442:369–75.
[5] van der Pijl EM, van Putten M, Niks EH, Verschuuren JJ, Aartsma-Rus A, Plomp JJ. Characterization of neuromuscular synapse function abnormalities in multiple Duchenne muscular dystrophy mouse models. Eur J Neurosci 2016;43:1623–35.
[6] Lyons PR, Slater CR. Structure and function of the neuromuscular junction in young adult mdx mice. J Neurocytol 1991;20:969–81.
[7] Brown JC, Charlton JE. Study of sensitivity to curare in certain neurological disorders using a regional technique. J Neurol Neurosurg Psychiatry 1975;38:34–45.
[8] Ihmsen H, Schmidt J, Schwilden H, Schmitt HJ, Muenster T. Influence of disease progression on the neuromuscular blocking effect of mivacurium in children and adolescents with Duchenne muscular dystrophy. Anesthesiology 2009;110:1016–19.
[9] Ririe DG, Shapiro F, Sethna NF. The response of patients with Duchenne's muscular dystrophy to neuromuscular blockade with vecuronium. Anesthesiology 1998;88:351–4.
[10] Tobias JD, Atwood R. Mivacurium in children with Duchenne muscular dystrophy. Paediatr Anaesth 1994;4:57–60.
[11] Tobias JD. Mivacurium administration in children with Duchenne muscular dystrophy. Anesth Analg 2000;90:498.
[12] Jirka S, Aartsma-Rus A. An update on RNA-targeting therapies for neuromuscular disorders. Curr Opin Neurol 2015;28:515–21.
[13] Aartsma-Rus A, Straub V, Hemmings R, Haas M, Schlosser-Weber G, Stoyanova-Beninska V, et al. Development of exon skipping therapies for Duchenne muscular dystrophy: a critical review and a perspective on the outstanding issues. Nucleic Acid Ther 2017;27:251–9.
[14] Alter J, Lou F, Rabinowitz A, Yin H, Rosenfeld J, Wilton SD, et al. Systemic delivery of morpholino oligonucleotide restores dystrophin expression bodywide and improves dystrophic pathology. Nat Med 2006;12:175–7.
[15] Lu QL, Mann CJ, Lou F, Bou-Gharios G, Morris GE, Xue SA, et al. Functional amounts of dystrophin produced by skipping the mutated exon in the mdx dystrophic mouse. Nat Med 2003;9:1009–14.
[16] Goemans NM, Tulinius M, van den Hauwe M, Kroksmark AK, Buyse G, Wilson RJ, et al. Long-term efficacy, safety, and pharmacokinetics of drisapersen in Duchenne muscular dystrophy: results from an open-label extension study. PLoS ONE 2016;11:e0161955.
[17] Mendell JR, Goemans N, Lowes LP, Alfano LN, Berry K, Shao J, et al. Longitudinal effect of eteplirsen versus historical control on ambulation in Duchenne muscular dystrophy. Ann Neurol 2016;79:257–71.
[18] Aartsma-Rus A, Krieg AM. FDA approves eteplirsen for Duchenne muscular dystrophy: the next chapter in the eteplirsen saga. Nucleic Acid Ther 2017;27:1–3.
[19] Matthews PM, Benjamin D, Van B I, Squier MV, Nicholson LV, Sewry C, et al. Muscle X-inactivation patterns and dystrophin expression in Duchenne muscular dystrophy carriers. Neuromuscul Disord 1995;5:209–20.
[20] Papa R, Madia F, Bartolomeo D, Trucco F, Pedemonte M, Traverso M, et al. Genetic and early clinical manifestations of females heterozygous for Duchenne/Becker muscular dystrophy. Pediatr Neurol 2016;55:58–63.
[21] Pegoraro E, Schimke RN, Garcia C, Stern H, Cadaldini M, Angelini C, et al. Genetic and biochemical normalization in female carriers of Duchenne muscular dystrophy: evidence for failure of dystrophin production in dystrophin-competent myonuclei. Neurology 1995;45:677–90.
[22] Soltanzadeh P, Friez MJ, Dunn D, von Niederhausern A, Gurvich OL, Swoboda KJ, et al. Clinical and genetic characterization of manifesting carriers of DMD mutations. Neuromuscul Disord 2010;20:499–504.
[23] Godfrey C, Muses S, McClorey G, Wells KE, Coursindel T, Terry RL, et al. How much dystrophin is enough: the physiological consequences of different levels of dystrophin in the mdx mouse. Hum Mol Genet 2015;24:4225–37.
[24] Li D, Yue Y, Duan D. Preservation of muscle force in Mdx3cv mice correlates with low-level expression of a near full-length dystrophin protein. Am J Pathol 2008;172:1332–41.
[25] van Putten M, Hulsker M, Nadarajah VD, van Heiningen SH, van Huizen E, van Iterson M, et al. The effects of low levels of dystrophin on mouse muscle function and pathology. PLoS ONE 2012;7:e31937.
[26] Newall AE, Duthie S, Formstone E, Nesterova T, Alexiou M, Johnston C, et al. Primary non-random X inactivation associated with disruption of Xist promoter regulation. Hum Mol Genet 2001;10:581–9.
[27] Karpati G, Zubrzycka-Gaarn EE, Carpenter S, Bulman DE, Ray PN, Worton RG. Age-related conversion of dystrophin-negative to -positive fiber segments of skeletal but not cardiac muscle fibers in heterozygote mdx mice. J Neuropathol Exp Neurol 1990;49:96–105.
[28] Weller B, Karpati G, Lehnert S, Carpenter S, Ajdukovic B, Holland P. Inhibition of myosatellite cell proliferation by gamma irradiation does not prevent the age-related increase of the number of dystrophin-positive fibers in soleus muscles of mdx female heterozygote mice. Am J Pathol 1991;138:1497–502.
[29] McLachlan EM, Martin AR. Non-linear summation of end-plate potentials in the frog and mouse. J Physiol 1981;311:307–24.
[30] Hulsker M, Verhaart I, van Vliet L, Aartsma-Rus A, van Putten M. Accurate dystrophin quantification in mouse tissue; identification of new and evaluation of existing methods. J Neuromuscul Dis 2016;3:77–90.
[31] Cirak S, Arechavala-Gomeza V, Guglieri M, Feng L, Torelli S, Anthony K, et al. Exon skipping and dystrophin restoration in patients with Duchenne muscular dystrophy after systemic phosphorodiamidate morpholino oligomer treatment: an open-label, phase 2, dose-escalation study. Lancet 2011;378:595–605.
[32] Goemans NM, Tulinius M, van den Akker JT, Burm BE, Ekhart PF, Heuvelmans N, et al. Systemic administration of PRO051 in Duchenne's muscular dystrophy. N Engl J Med 2011;364:1513–22.
[33] Li D, Yue Y, Duan D. Marginal level dystrophin expression improves clinical outcome in a strain of dystrophin/utrophin double knockout mice. PLoS ONE 2010;5:e15286.

[34] van Putten M, Hulsker M, Young C, Nadarajah VD, Heemskerk H, van der Weerd L, et al. Low dystrophin levels increase survival and improve muscle pathology and function in dystrophin/utrophin double-knockout mice. FASEB J 2013;27:2484–95.

[35] Scarlato G, Valli G, Meola G, Carenini L. Quantitative EMG and histological carrier detection of Duchenne muscular dystrophy. J Neurol 1977;216:235–49.

[36] Toulouse P Coatrieux JL, LeMarec B. An attempt to differentiate female relatives of Duchenne type dystrophy from healthy subjects using an automatic EMG analysis. J Neurol Sci 1985;67:45–55.

[37] Bruusgaard JC, Liestol K, Ekmark M, Kollstad K, Gundersen K. Number and spatial distribution of nuclei in the muscle fibres of normal mice studied in vivo. J Physiol 2003;551:467–78.